



Eco-friendly synthesis of nano ferrites for effective dye degradation and enhanced antimicrobial protection

Manikandan Dhayalan^a, Rathika Govindasamy^{b,*}, Karthikeyan Prakasham^c, Moonis Ali Khan^d, Anuchit Phanumartwiwath^{a,*}

^a College of Public Health Sciences, Chulalongkorn University, Bangkok 10330, Thailand

^b Department of Chemistry, PSG College of Arts & Science, Coimbatore 641014, Tamil Nadu, India

^c Research Center for Precision Environmental Medicine, and Ph.D. Program in Environmental and Occupational Medicine, College of Medicine, Kaohsiung Medical University, Kaohsiung City, Taiwan

^d Chemistry Department, College of Science, King Saud University, Riyadh 11451, Saudi Arabia

ARTICLE INFO

Keywords:

Araucaria heterophylla
Catalyst
Reduction
Methylene blue
Rhodamine- B

ABSTRACT

This study investigates the synthesis of cobalt and nickel ferrite NPs using *Araucaria heterophylla* resin as a biotemplate and nitrate salts of cobalt, nickel, and iron as precursors. The resulting spinel systems exhibit efficient degradation of organic dyes, including methylene blue and rhodamine-B, and demonstrate excellent reusability. The NPs antibacterial efficacy against pathogenic bacteria, such as *Staphylococcus aureus*, *Bacillus subtilis*, *Escherichia coli*, and *Salmonella paratyphi*, was also evaluated. Comprehensive characterization of the nano-materials was performed using FT-IR, XRD, SEM, TEM, EDX, and VSM techniques. Magnetic measurements revealed the ferromagnetic nature of cobalt ferrites and the superparamagnetic nature of nickel ferrites, with reduced saturation magnetization and coercivity compared to bulk materials due to the quantum size effect. The nano-formulated ferrites exhibited superior antibacterial activity, highlighting their potential for water treatment applications. This study underscores the importance of removing dye contaminants from wastewater before discharge into aquatic ecosystems.

1. Introduction

Nanoparticles (NPs) have garnered significant attention in catalytic, energy, medicinal, and materials science research due to their unique chemical and physical properties (Tiekink 2002, Nam et al., 2009). Their physiochemical, optical, and electronic attributes are profoundly influenced by dimensions, structure, and surface topology. Traditional metallic NP synthesis methods include sol-gel, ultra-sonication, electrochemical synthesis, hot spraying, physical vapor deposition (PVD), chemical reduction of metallic ions, and microwave-assisted synthesis (Byun et al., 2000, Sarkar et al., 2017, Zou et al., 2017, Chung and Zhang 2021, Vorobyova et al., 2023, Pedone et al., 2005). However, these methods often employ ecologically hazardous chemicals and reagents. Recently, eco-friendly approaches utilizing microorganisms and plant-based extracts have emerged as viable alternatives for NP synthesis, offering a facile and environmentally sustainable solution (Al-Farraj et al., 2018, Laghrib et al., 2019, Patil and Behera 2023, Masuku et al., 2024).

Nanomaterials based on 3D transition metal oxides (Fe_3O_4 , $\alpha\text{-Fe}_2\text{O}_3$, $\gamma\text{-Fe}_2\text{O}_3$, CoO , Co_3O_4 , and NiO) and mixed metal oxides (CoFe_2O_4 , NiFe_2O_4 , and MnFe_2O_4) have demonstrated potential in catalytic, medical, and various research applications. Notably, plant extracts have emerged as effective biotemplates for synthesizing NPs with enhanced surface area and stability. Specifically, extracts from kobushi magnolia (Mokryeon), kaki persimmon (Japanese persimmon), and *Ficus indica* (banyan) have been shown to produce highly stable NPs (Prathna et al., 2011, Dhayalan et al., 2018, Shanmugam et al., 2022). This stability is attributed to the presence of bioactive compounds, including flavonoids, polyphenols, and alkaloids, which serve as reducing agents in plant extracts.

The synthesis and application of functional metal ferrites have garnered significant attention in recent years due to their exceptional magnetic properties. Notably, their superparamagnetic nature enables effortless separation from reaction mixtures, eliminating the need for tedious and prolonged separation steps (Ranjithkumar et al., 2014). Consequently, researchers have leveraged ferrite NPs to address various

* Corresponding authors.

E-mail addresses: rathikapsgcas@gmail.com (R. Govindasamy), anuchit.p@chula.ac.th (A. Phanumartwiwath).

<https://doi.org/10.1016/j.jksus.2024.103466>

Received 19 July 2024; Received in revised form 24 September 2024; Accepted 25 September 2024

Available online 26 September 2024

1018-3647/© 2024 The Author(s). Published by Elsevier B.V. on behalf of King Saud University. This is an open access article under the CC BY-NC-ND license (<http://creativecommons.org/licenses/by-nc-nd/4.0/>).

challenges, including water contamination treatment, sensor development, and antibacterial applications. Previous studies have demonstrated the versatility of cobalt ferrite NPs in oxidizing carbamazepine. (He et al., 2017) targeting human ferritin cancer cells. (Leonel et al., 2021) and detecting NO₂ gas (Bagade et al., 2017) Similarly, magnetically recoverable NiFe₂O₄ NPs have been synthesized for reducing nitroarenes (Zeynizadeh et al., 2017) and explored for magnetic resonance imaging (MRI), target drug delivery, and controlled drug release applications. (Wu et al., 2011, Koul et al., 2021)

The widespread use of synthetic dyes, such as methylene blue and rhodamine-B, in various industries poses significant environmental risks (Alfryyan et al., 2022). The discharge of untreated industrial wastewater containing these dyes into water bodies deteriorates water quality and potentially harms human health and aquatic ecosystems. Due to their mutagenic and carcinogenic properties, efficient treatment strategies are crucial to remove or degrade dye contaminants from industrial effluents. (McMullan et al., 2001, Wang et al., 2018, Jara et al., 2024) In response, governments in developed countries have implemented strict environmental regulations. Currently, industries are focusing on synthesizing efficient catalysts using cost-effective, eco-friendly materials to reduce dye concentrations. This effort aligns with the United Nations Sustainable Development Goal (SDG) 6.3, aiming to improve water quality by 2030 through reduced pollution, elimination of harmful chemicals, and increased wastewater treatment and safe reuse globally (Chirgwin et al., 2021).

A clean and green calcination method was developed to synthesize cobalt and nickel ferrite nanomaterials using *Araucaria heterophylla* resin as a sustainable biotemplate (Scheme 1). The synthesized ferrites were subjected to a thorough characterization, including X-ray diffraction, scanning electron microscopy, transmission electron microscopy, energy-dispersive X-ray spectroscopy, and vibrating sample magnetometry, to elucidate their structural, morphological, chemical, elemental, and magnetic properties. Additionally, their photocatalytic efficiency and antibacterial efficacy were assessed through standardized assays.

2. Experimental

2.1. Materials

Analytical-grade chemicals were used throughout the study. Iron(III) nitrate nonahydrate (Fe(NO₃)₃•9H₂O), cobalt(II) nitrate hexahydrate (Co(NO₃)₂•6H₂O), nickel(II) nitrate hexahydrate (Ni(NO₃)₂•6H₂O), sodium hydroxide (NaOH), hydrochloric acid (HCl), methylene blue (MB), and rhodamine-B (RhB) were purchased from Sigma Aldrich (Mumbai, India).

2.2. Preparation of *Araucaria heterophylla* resin extract

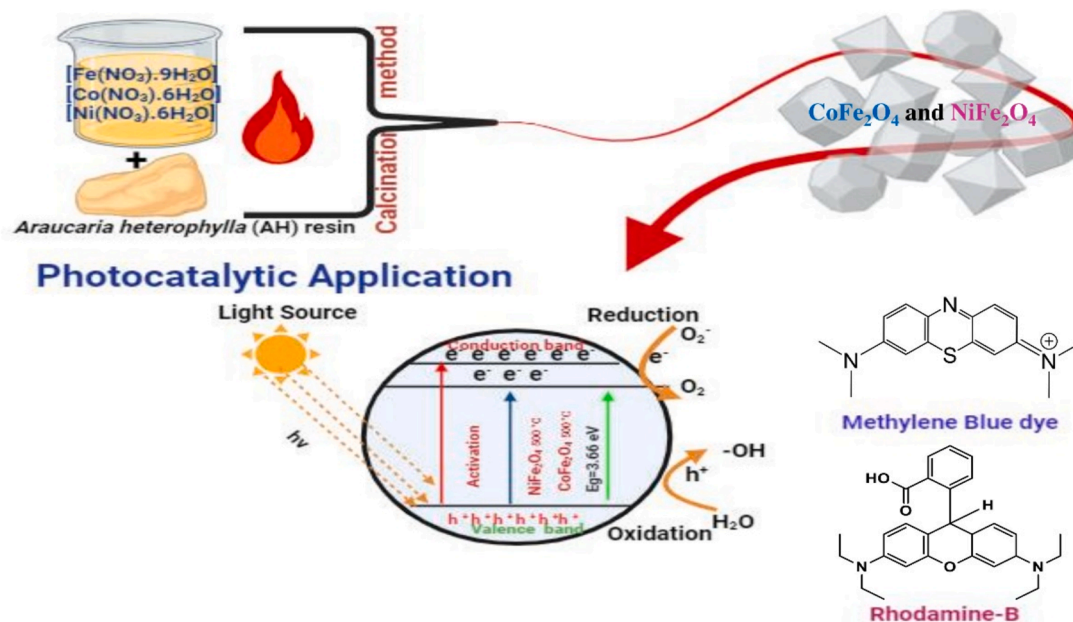
The collected *A. heterophylla* (AH) resin was cleaned with double-distilled water. A stock solution (1000 mg/L) was prepared by dissolving 1 g of AH resin in 1000 mL of double-distilled water.

2.3. Synthesis of Cobalt and Nickel Ferrite Nanoparticles

Cobalt ferrite NPs were synthesized by mixing 2 M iron(III) nitrate (10 mL) and 1 M cobalt(II) nitrate (10 mL) solutions (Fe³⁺:Co²⁺ ratio of 2:1). The mixture was mechanically agitated for 30 min at room temperature and then added to a boiling 1000 mg/L AH resin extract solution (100 mL) under continuous agitation. The resulting brown precipitate was filtered (Whatman No. 1 filter paper), dried at room temperature, and calcined at 600 °C. Nickel ferrite NPs were synthesized using an identical protocol with 2 M iron(III) nitrate (10 mL) and 1 M nickel(II) nitrate (10 mL) solutions (Fe³⁺:Ni²⁺ ratio of 2:1).

2.4. Characterization of cobalt and nickel ferrite nanoparticles

The synthesized cobalt and nickel ferrite NPs were characterized using various analytical techniques. Scanning electron microscopy (SEM, JSM 6390 LV) coupled with energy-dispersive X-ray analysis (EDX) determined the morphological and chemical characteristics of the ferrite NPs. Fourier transform infrared spectroscopy (FT-IR, JASCO FT/IR-4600) identified the chemical functionalities on the nanoparticle surfaces. The crystalline structure and size of the ferrite NPs were analyzed using X-ray Diffraction (XRD, Shimadzu X-ray machine 6000) with Cu K α radiation ($\lambda = 0.1548$ nm) at 40 kV and 80 mA, scanning 2 θ from 10° to 90°. High-Resolution Transmission Electron Microscopy (HRTEM, Talos F200X G2) and Selected Area Electron Diffraction (SAED, Technai G20-stwin) at 200 kV accelerating voltage provided insights into the size, morphology, and crystal nature of the ferrite NPs.



Scheme 1. Green synthesis of CoFe₂O₄ and NiFe₂O₄ Nanoparticles.

2.5. Catalytic degradation of synthetic dyes

Cobalt and nickel ferrite NPs were evaluated for catalytic degradation of methylene blue (MB) and rhodamine-B (RhB) dyes at room temperature (Jara et al., 2024). A 2 mL dye solution (20 mg/L) was treated with 10 mg of ferrite NPs. The reaction progress was monitored using a UV-visible spectrophotometer after adding 1 mL of a 10 mg/L NaBH_4 solution. The maximum wavelengths for MB and RhB were at 660 nm and 554 nm, respectively. After completion, the solid and solution phases were separated using an external electromagnet. The recovered catalyst was washed, dried, and reused.

2.6. Antibacterial activity

The antibacterial activity of cobalt and nickel ferrite NPs was assessed using the agar-based well diffusion method (Dhayalan et al., 2018). Gram-positive bacteria (*Staphylococcus aureus* MTCC 87, *Bacillus subtilis* MTCC1134) and gram-negative bacteria (*Escherichia coli* MTCC40, *Salmonella paratyphi* MTCC735) were employed. Overnight cultures were spread on nutrient agar medium (pH 6.8) and incubated at 37°C. Cobalt and nickel ferrite NPs (100 μg) were loaded into 6 mm-diameter wells. After 24-hours incubation at 37°C, the zones of inhibition (ZOI) were measured. The results were compared with a positive control (Ciprofloxacin 10 $\mu\text{g}/\text{mL}$) and a negative control (D.I. water) (Shanmugam et al., 2022). The experiment was run in triplicate.

3. Results and discussion

Fourier Transform Infrared (FT-IR) spectroscopy was employed to investigate the surface composition of synthesized NPs. This analysis revealed specific functional groups involved in NPs formation, shedding light on interactions between metal ions (cobalt and nickel ferrite) and phytochemicals from plant extracts. (Chirgwin et al., 2021, McMullan et al., 2001) The FT-IR spectrum of AH gum extract displayed characteristic bands at 3360.35 cm^{-1} (O-H stretching), 2913.26 cm^{-1} (C-H/CH₂ vibrations), 1644 cm^{-1} (C=C stretching), 1375 cm^{-1} (C-O stretching), and 1020 cm^{-1} (C-O bonds) (Fig. 1a). Comparison of FT-IR spectra for AH-bound metal nitrates (Fig. 1a, c) and corresponding ferrite NPs (Fig. 1b, d) revealed distinct peak patterns. The AH-bound metal nitrates exhibited numerous peaks between $1000\text{--}3000\text{ cm}^{-1}$, indicating various active functional groups from the AH biopolymer. Peaks at $555/462\text{ cm}^{-1}$ (Fig. 1a) and $486/584\text{ cm}^{-1}$ (Fig. 1c) arose from bond formation between AH biopolymer and metal nitrates. In contrast, ferrite NPs (Fig. 1b, d) showed no characteristic peaks in this region. Firm peaks at $458/540\text{ cm}^{-1}$ (Fig. 1b) and $452/630\text{ cm}^{-1}$ (Fig. 1d) indicated cobalt and nickel ferrite formation. FT-IR analysis confirmed

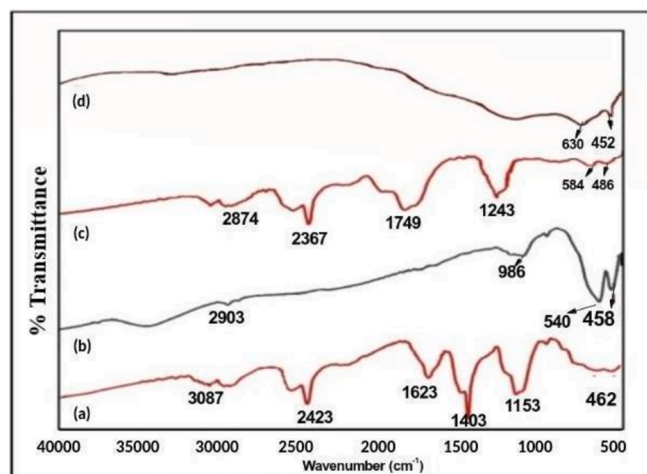


Fig. 1. FT-IR spectra of CoFe_2O_4 and NiFe_2O_4 precursors and NPs.

complete decomposition of AH biopolymer extracts during calcination at 600°C. (Hajdu et al., 2022, Passero et al., 2024) The band shift in FT-IR spectra suggested interactions between extract compounds and metal ions during NP construction. Soluble extract components possibly acted as capping agents, preventing FeNP aggregation. (Ahmed et al., 2020, Hajdu et al., 2022).

XRD patterns are frequently used to study the phase structure of the various nanocatalysts. The powdered XRD (PXRD) patterns of cobalt ferrite and nickel ferrite are illustrated in (Fig. 2a1 and 2a2 respectively). The JCPDS card numbers 22-1086 nicely match the seven sharp peaks (111, 220, 311, 400, 511, 620, and 533) seen in (Fig. 2a1). Similarly, (Fig. 2a2) displays five distinct peaks that match the JCPDS card no. 03-0875 (220, 311, 400, 511, and 440). The production of cobalt and nickel ferrite NPs in their cubic spinel structure was confirmed by the JCPDS card results. (Ahmed et al., 2020, Alzoubi 2022) Using XRD data and the Scherrer equation, the typical crystallite structure was 7 nm for cobalt ferrite and 11 nm for nickel ferrite, and these results were also in agreement with TEM results (Fig. 2b).

The study utilized TEM to visualize the size and morphology of the cobalt and nickel ferrite NPs. TEM images displayed the broken pieces of rock of the NPs with higher aggregation, which were evenly distributed. The crystalline size of cobalt ferrite and nickel ferrite was found to be < 10 nm. The TEM images of cobalt and nickel ferrite NPs are presented in (Fig. 2b). The powdered XRD data's Full width at half maximum (FWHM) value agreed with the TEM findings. Moreover, the occurrence of diffraction rings and perky spots in the selected area electron diffraction (SAED) pattern indicated that the produced ferrite NPs were highly crystalline, as shown in (Fig. 2a). The nine diffraction peaks that were seen for Co and Ni ferrite NPs (220, 111, 400, 422, 311, 511, 620, 533, and 642 in (Fig. 2a1), and 220, 311, 400, 511, and 440 in (Fig. 2a2) match the JCPDS card numbers 22-1086 and 03-0875 quite well. The production of Co/Ni Fe_2O_4 NPs with a cubic spinel shape was confirmed by the JCPDS card results. Compared to the SAED pattern of the produced ferrite NPs, the PXRD pattern yielded the same results. (Londono-Calderon et al., 2017, Khoso et al., 2021).

Scanning electron microscopy (SEM) was employed to investigate the surface morphology of cobalt and nickel ferrite catalysts (Fig. 3). The micrographs revealed irregular, rock-like structures with significant agglomeration, attributed to steric effects and magnetic interactions between ferrite NPs. The magnetic dipole-dipole interactions likely caused NPs to attract and aggregate. Complementary energy-dispersive X-ray analysis (EDAX) spectra (Fig. 3) confirmed the atomic composition of cobalt and nickel ferrite catalysts, displaying a 1:2:4 ratio of Co/Ni:Fe:O. This ratio corroborates the successful synthesis of cobalt and nickel ferrite catalysts using AH biopolymer extract. The SEM and EDAX results provide valuable insights into the morphology and composition of the ferrite catalysts, informing the development of efficient and effective catalysts for various applications.

The magnetic characteristics of cobalt and nickel ferrite NPs were investigated at room temperature using a vibrating sample magnetometer with a 10 kOe applied field (Supplementary Fig. 1). The hysteresis loops yielded saturation magnetization (M_s), remanence (M_r), and coercive force (H_c) values (Table 1). Compared to bare cobalt ferrite ($M_s = 94\text{ emu/g}$). (Sadeghi et al., 2020) and bare nickel ferrite ($M_s = 19\text{ emu/g}$) (Yelgaonkar et al., 2020) the magnetic parameters of cobalt and nickel ferrite NPs decreased, consistent with reduced NP size. The ferromagnetic behavior was confirmed by the M_r/M_s ratio (Supplementary Table 1), indicating that cobalt ferrite NPs exhibited ferromagnetism, while nickel ferrite NPs displayed superparamagnetic behavior at room temperature, with M_r/M_s ratios < 25%. (Tandon et al., 2021, Sofronice et al., 2022, Dippong et al., 2023).

3.1. Optimization of the dye degradation process

The discharge of persistent industrial pollutants, including dyes, nitroarenes, pharmaceuticals, and cosmetics, deteriorates surface and

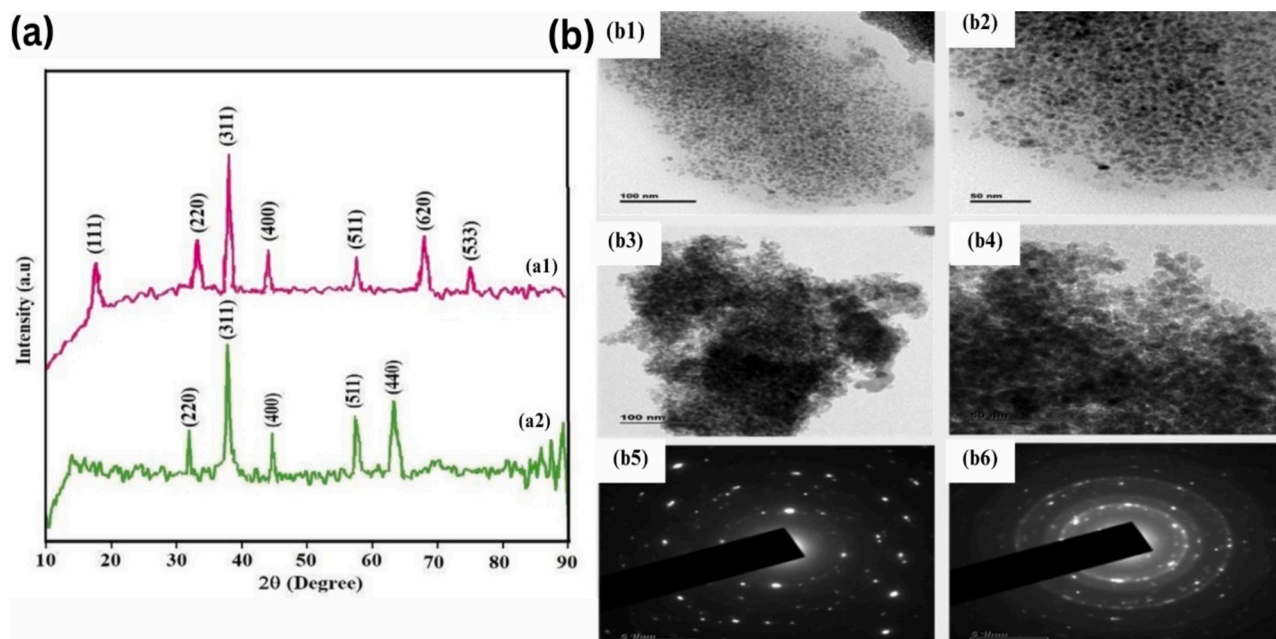


Fig. 2. XRD patterns (a1, a2) and TEM images of CoFe_2O_4 , NiFe_2O_4 (b1-6).

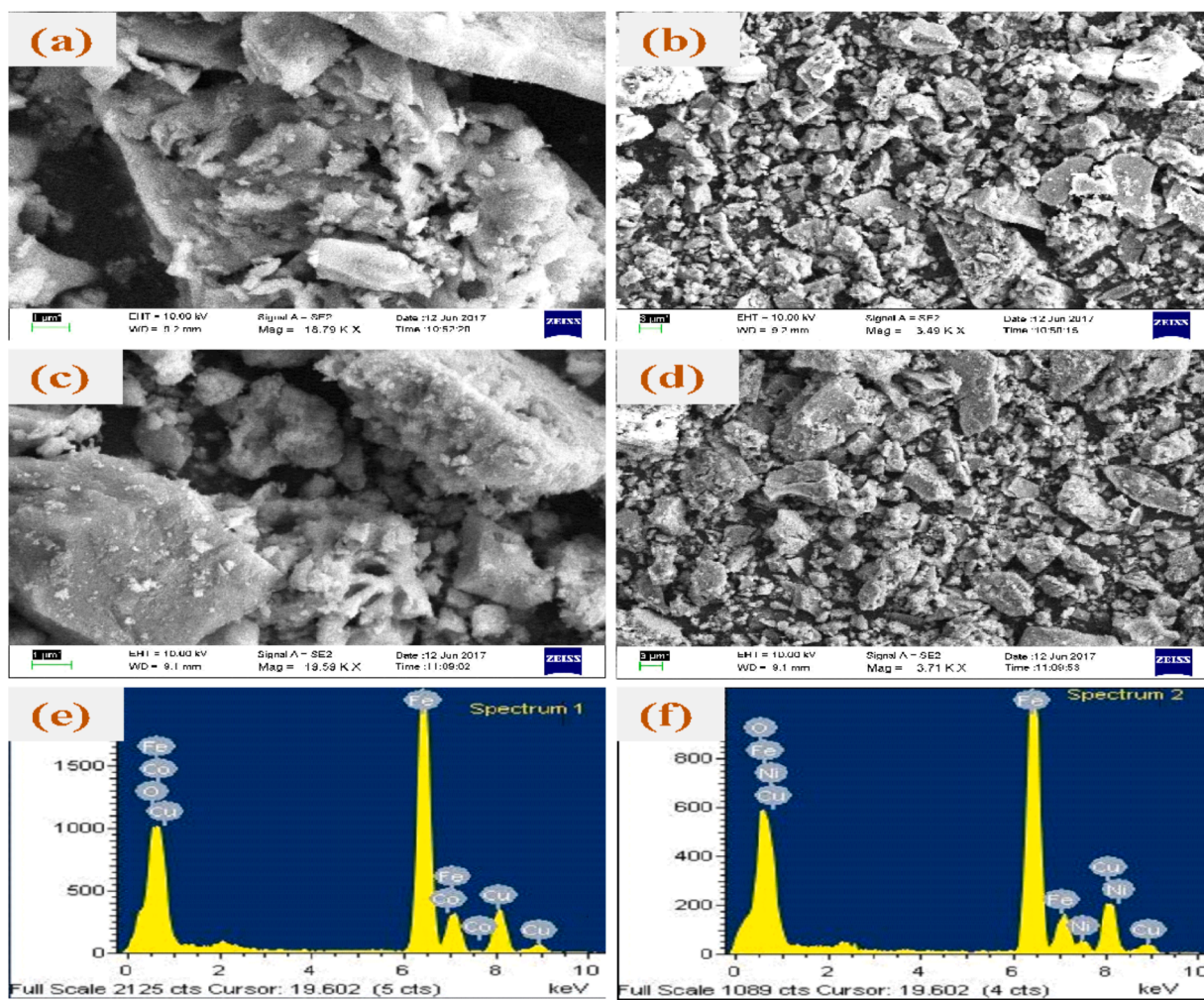


Fig. 3. SEM images (a-d) and EDAX spectra of (e) CoFe_2O_4 and (f) NiFe_2O_4 .

Table 1
Comparative catalytic activity of CoFe₂O₄/NiFe₂O₄ NPs in MB/RhB degradation.

Catalyst	Reaction condition	MB/RhB	Time (min)	Ref
Graphene/Au	0.01 mM of 1 mL dye + 1 mL of 0.01 mM NaBH ₄	MB	10	(Zou et al., 2017)
Ag NPs	10 mM of 10 mL dye + 1 mM of 3 mL NaBH ₄	MB	10	(Dhayalan et al 2018)
Ag-Fe ₃ O ₄ @PDA	7.5 mg/L of 20 mL dye + 0.1 M of 0.5 mL NaBH ₄ .	MB	30	(Hajdu et al., 2022)
CaFe ₂ O ₄ /g-C ₃ N ₄	10 mg/L of 50 mL Dye + UV radiation	MB	120	(Alzoubi et al., 2022)
CoFe ₂ O ₄	20 ppm of 2 mL dye + 10 mM of NaBH ₄	MB	27	This PresentStudy
NiFe ₂ O ₄	20 ppm of 2 mL dye + 10 mM of NaBH ₄	MB	30	This PresentStudy
Au NPs	5 × 10 ⁻⁵ M of 2 mL dye + 0.006 M of NaBH ₄	RhB	5	(Zou et al., 2017)
Ag NPs	5 × 10 ⁻⁵ M of 2 mL Dye + 0.006 M of NaBH ₄	RhB	9	(Shanmugam et al., 2022)
Au-pTA	10 ⁻⁴ mol dm ⁻³ of 2.5 mL+Proton transfer by PCET method	RhB	10	(Devarajan et al., 2005)
CoFe ₂ O ₄	20 ppm of 2 mL dye + 10 mM of NaBH ₄	RhB	20	This PresentStudy
NiFe ₂ O ₄	20 ppm of 2 mL dye + 10 mM of NaBH ₄	RhB	9	This PresentStudy

subsurface water quality, posing significant risks to human and environmental health. Ferrite NPs have emerged as effective heterogeneous catalysts for removing water-borne dye pollution (Bagade et al., 2017, Jara et al., 2024). To mitigate these harmful effects, efficient removal of these pollutants is crucial. The degradation of dyes can be achieved through reduction using mild reducing agents. Sodium borohydride (NaBH₄) is a commonly employed reducing agent for this purpose. The reduction mechanism involves the transfer of hydride ions (H⁻) from NaBH₄ to the dye solution, breaking down large dye molecules into smaller, less toxic fragments (Jara et al., 2024).

3.1.1. Optimization of NaBH₄ concentration

NaBH₄ was selected as the reducing agent due to its mild, selective, and eco-friendly properties. Its non-toxicity, non-flammability, and ease of handling make it an ideal choice for dye degradation. To optimize the degradation process, experiments were conducted using 5 mg of CoFe₂O₄ catalyst with varying NaBH₄ concentrations (1–14 mM). Results (Fig. 4a, b) showed maximum degradation of RhB and MB dyes at 10 mM and 12 mM NaBH₄, respectively. Similarly, using NiFe₂O₄ catalyst, optimal degradation was achieved at 9 mM (RhB) and 11.5 mM (MB) NaBH₄ concentrations.

3.1.2. Optimization of catalyst amount

The effectiveness of a catalyst in dye degradation is dependent on the amount of catalyst used, as it directly impacts the surface area of the catalyst available for the reaction. A higher surface area of the catalyst can lead to more active sites for the reaction, resulting in more effective degradation of dyes. On the other hand, using too much catalyst can result in agglomeration, which reduces the surface area accessible for the reaction and, in turn, hinders the efficacy of the catalyst. Furthermore, the amount of catalyst used can also affect the reaction kinetics. For instance, too little catalyst may reduce the reaction rate, leading to incomplete dye degradation. At the same time, too much catalyst may cause the reaction to proceed too quickly, leading to incomplete degradation. Therefore, it is essential to optimize the amount of catalyst used for the reaction to achieve the desired degradation efficiency and minimize cost. Therefore, in the present work, the amount of ferrite NPs was varied from 2.5 to 20 mg, tested for 30 min using a 10 mM concentration of NaBH₄ for the degradation of MB and RhB. The results depicted in (Fig. 4 c) clearly showed that 10 mg of catalysts exhibited the maximum degradation of MB and RhB, and it remained constant at 15 mg of catalyst. When increasing the catalyst amount to more than 15 mg, dye degradation is lessened due to the accessibility of less energetic surface area on the catalyst surface due to agglomeration.

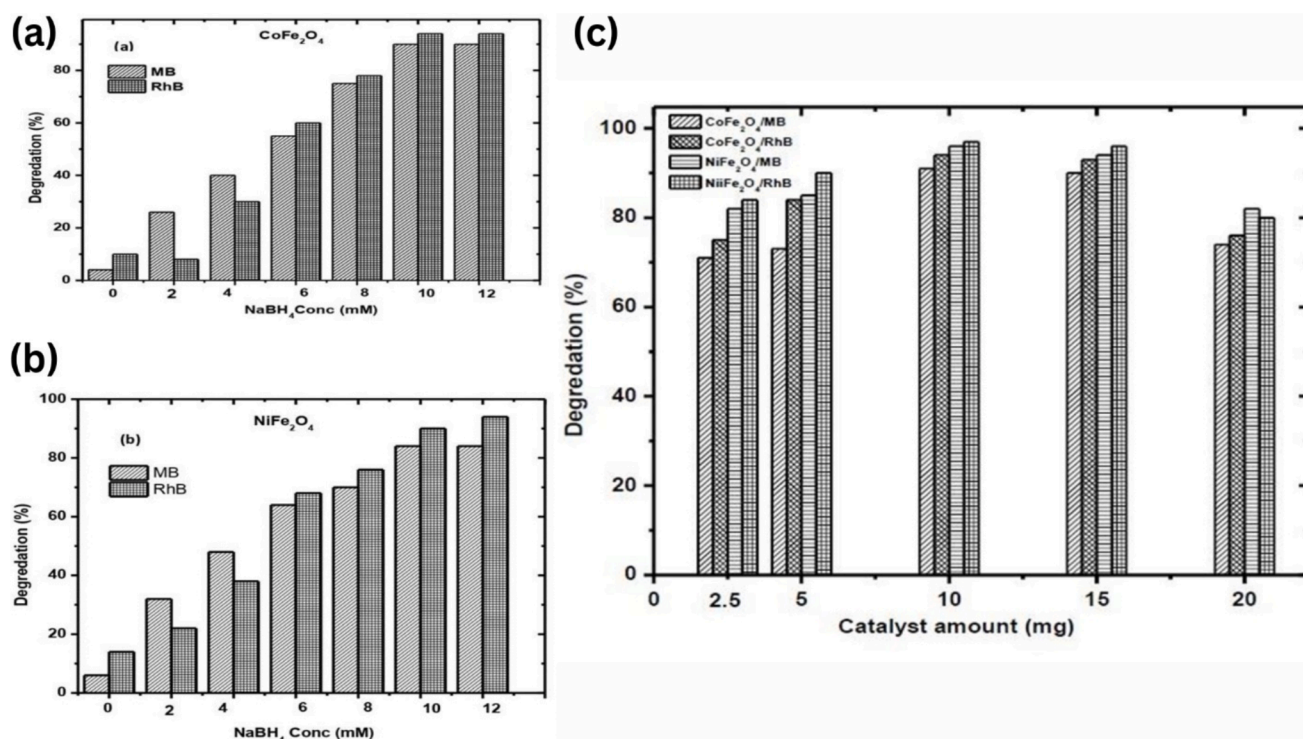


Fig. 4. Effect of NaBH₄ concentration (4a-b) and catalyst amount on MB/RhB degradation (4c).

3.1.3. Optimization of contact time

During the experiment, a dye solution (2 mL) of 20 mg/L initial concentration was treated with 10 mg of ferrite catalyst and 10 mM NaBH₄ at varied contact time range (0 to 40 min). Results showed that the maximum degradation of MB by CoFe₂O₄ and NiFe₂O₄ NPs was observed at 25 min and 30 min contact times, respectively. While maximum RhB degradation by CoFe₂O₄ and NiFe₂O₄ NPs was observed at 20 min and 10 min, respectively, as illustrated in (Fig. 5) The absorbance bands presented in (Fig. 6a and 6b) at varied contact times affirmed the results for dyes degradation. Comparative results our study show that nickel ferrite catalyst exhibited a 97% better degradation against RhB dye within 10 min under the studied experimental conditions (Fig. 7).

3.1.4. Kinetic modelling for dyes reduction

Pseudo-first-order and pseudo-second-order kinetic models in linearized forms were practical to MB and RhB degradation data by CoFe₂O₄ and NiFe₂O₄ NPs. The best-fitted model was decided to be constructed on higher regression coefficient (R²) value.

The pseudo-first order and the pseudo-second-order kinetic models are given by expressions:

Pseudo-first order model:

$$\log(q_e - q_t) = \log q_e - \frac{k_1 t}{2.303} \dots \quad (1)$$

Pseudo-second order model:

$$\frac{t}{q_t} = \frac{1}{k_2 q_e^2} + \frac{t}{q_e} \dots \quad (2)$$

Where t is the reduction process's time (min), q_e and q_t are the amounts of MB and RhB condensed (mg/L) at any time t and at equilibrium, and k_1 (1/min) and k_2 (g/mg-min) are the pseudo-first and second-order rate constants, correspondingly. (Supplementary Table 2) lists the R² values, and (Supplementary Fig. 2) displays their plot. For CoFe₂O₄ and NiFe₂O₄ NPs, the data fitted well to pseudo-second-order kinetic model.

3.1.5. Mechanism of reduction process

The reduction of MB and RhB in the presence of NaBH₄ and the synthesized ferrite catalyst NPs at room temperature have been studied. After being treated with NaBH₄ and a catalyst, the colors of the MB and RhB solutions instantly turn colorless. It is understood that the catalytic reaction occurred in the existence of ferrite NPs by an electron transfer and by an electrochemical mechanism in which nucleophile BH₄⁻ ions

donate electrons to electrophilic organic MB and RhB concluded ferrite NPs. After the chemisorption of dyes and BH₄⁻ on their surfaces, synthesized ferrite NPs were allowed for electron transport, which speeds up the reduction of dyes. Consequently, after being treated with NaBH₄, the dye solution, including NPs, was completely discolored. This result demonstrates how quickly and completely MB and RhB can be converted by ferrite NPs to their colorless leuco form. (Jara et al., 2024).

3.1.6. Stability and reuse of ferrite catalysts

The NPs' recovery was evaluated using an external magnet by the exclusion of nanocatalysts from the reaction mixture (Supplementary Fig. 3). The catalyst was observed to be drawn to the magnet and adhered to the magnet's surface, making the solution transparent and easily removed by decanting the colorless solution. It can be utilized as a magnetic catalyst to lessen the dye pollution in aqueous solutions. The findings in (Fig. 8) provide information about the catalytic behavior of recovered materials utilized for more cycles after being rinsed with ethanol, acetone, and water, dried, and reused even after up to four additional runs. These also confirm the catalytic behavior of synthesized catalysts without any loss of activity by reducing almost 90% of both dyes (MB and RhB).

3.2. Antibacterial activity of cobalt and nickel ferrite nanoparticles

Along with regular ciprofloxacin, the in vitro antibacterial properties of CoFe₂O₄ and NiFe₂O₄ NPs have been examined, as shown in (Supplementary Fig. 4). Gram-negative bacteria (*E. coli* and *S. paratyphi*) and Gram-positive bacteria (*S. aureus* and *B. subtilis*) are used in this study's investigation. Here, the inhibition zone of CoFe₂O₄ and NiFe₂O₄ NPs was measured to assess their bactericidal capabilities against the aforementioned microorganisms. When the results from (Supplementary Table 3) are analyzed, the CoFe₂O₄ exhibits a very strong bacterial inhibition zone. It was learned that both utilized bacterial species are responsive to the active ferrite NPs.

3.3. Advantages and disadvantages of the present study

This study presents a highly efficient method for methylene blue (MB) and rhodamine B (RhB) dye degradation using CoFe₂O₄ and NiFe₂O₄ nanocatalysts synthesized via green biopolymer extraction. The proposed method offers several advantages, including optimal dye concentration, shorter reaction times (compared to Table 1), flexibility in catalyst selection, and the introduction of novel, cost-effective catalysts. However, considerations include potential influences of dye type, concentration, pH, and temperature on catalyst performance, as well as the requirement for thorough catalyst characterization to ensure stability and efficacy. Despite these limitations, this comprehensive evaluation provides valuable insights for researchers and practitioners in the field of dye degradation, contributing significantly by evaluating a range of catalysts and highlighting their advantages and disadvantages.

4. Conclusions

The current study has covered a straightforward, environmentally friendly process for creating stable magnetic ferrite NPs without hazardous chemicals. Other transition and rare earth metal oxides can be treated using this technique. Ferrite NPs have very small magnetic characteristics. In addition, there is a permanent magnet in aqueous media. The degradation of MB and RhB is appropriate aimed at the pseudo-second-order model. Our findings demonstrate that transition metal-substituted cobalt ferrite NPs possess enhanced antibacterial activity against *E. coli*, outperforming the other three compounds assessed. Given their unique properties, ferrite NPs have significant potential for exploitation in various biomedical and biotechnological contexts, including the development of targeted drug delivery platforms and efficient catalytic systems.

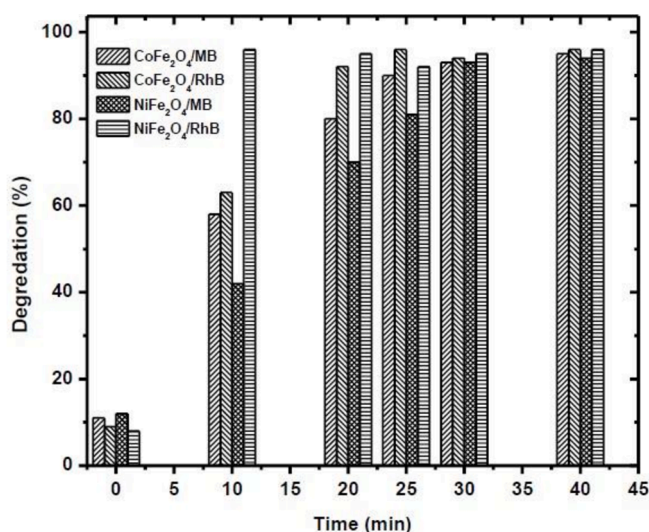


Fig. 5. Time-dependent degradation of MB/RhB using CoFe₂O₄/NiFe₂O₄.

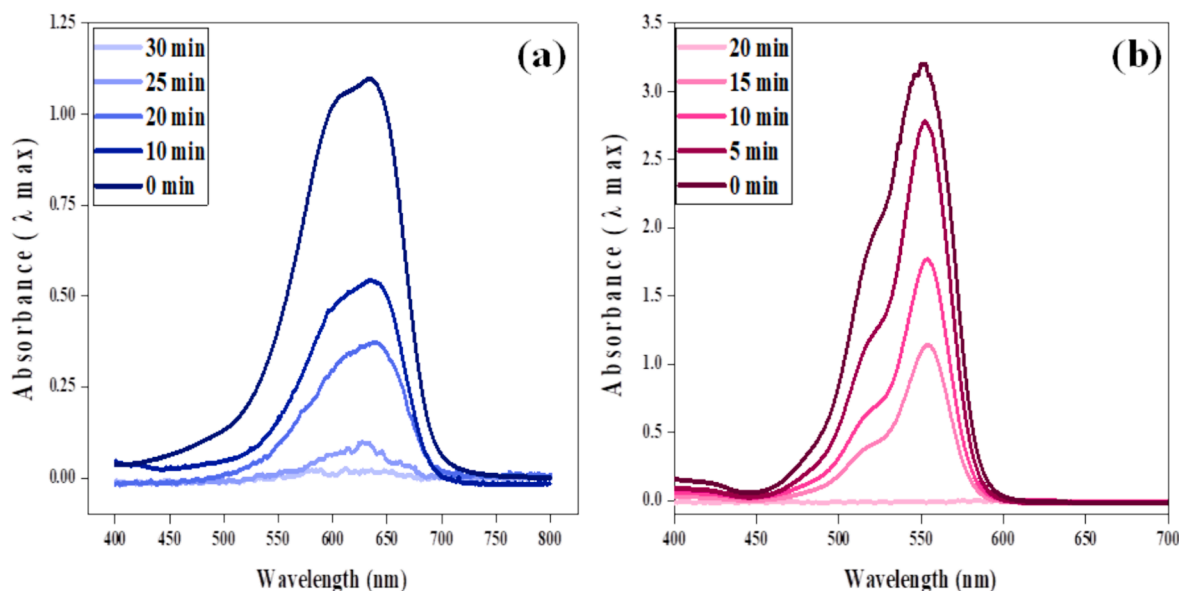


Fig. 6. Electronic band structure during MB/RhB reduction.

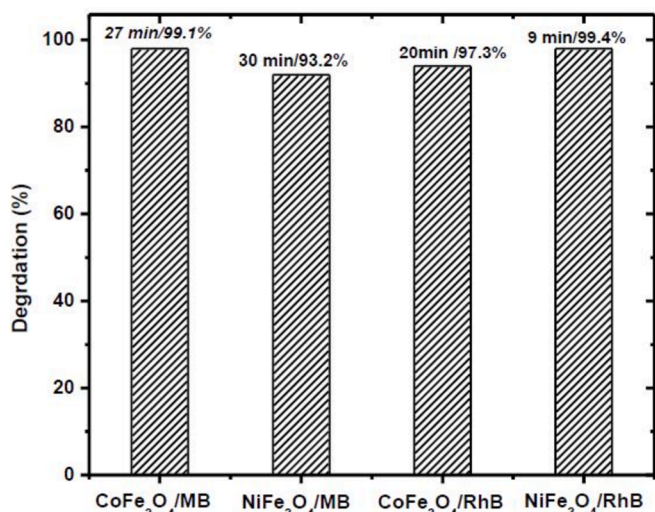


Fig. 7. Removal efficiency of MB/RhB using CoFe₂O₄/NiFe₂O₄.

CRedit authorship contribution statement

Manikandan Dhayalan: Writing – review & editing, Writing – original draft, Validation, Supervision, Resources, Project administration, Methodology, Investigation, Funding acquisition, Formal analysis, Data curation, Conceptualization. **Rathika Govindasamy:** Writing – review & editing, Writing – original draft, Supervision, Software, Resources, Project administration, Methodology, Investigation, Data curation, Conceptualization. **Karthikeyan Prakasham:** Writing – review & editing, Supervision, Investigation, Funding acquisition, Conceptualization. **Moonis Ali Khan:** Writing – review & editing, Supervision, Project administration, Funding acquisition, Formal analysis. **Anuchit Phanumartwiwath:** Writing – review & editing, Writing – original draft, Visualization, Validation, Supervision, Methodology, Investigation, Funding acquisition, Formal analysis, Data curation, Conceptualization.

Declaration of competing interest

The authors declare that they have no known competing financial

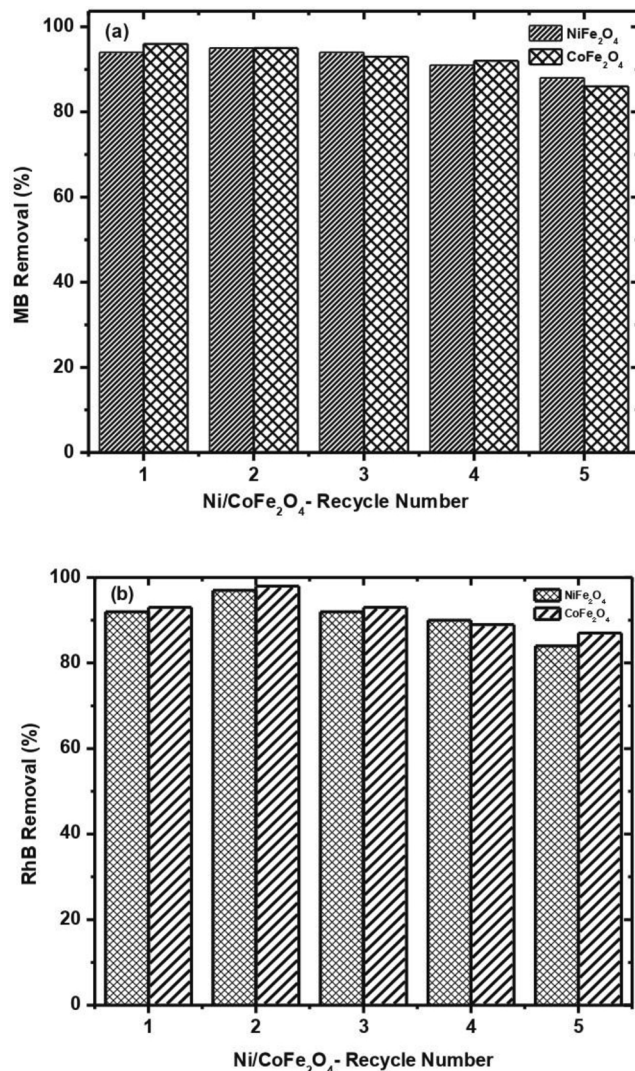


Fig. 8. Recycling capability of NiCoFe₂O₄ NPs for MB/RhB degradation.

interests or personal relationships that could have appeared to influence the work reported in this paper.

Acknowledgments

This research project is supported by Second Century Fund (C2F) from Chulalongkorn University (CU). Manikandan Dhayalan (M.D) is thankful to C2F for postdoctoral fellowship.

Moonis Ali Khan acknowledges the financial support through Researchers Supporting Project number (RSP2024R345), King Saud University, Riyadh. Saudi Arabia.

Funding

Moonis Ali Khan acknowledges the financial support through Researchers Supporting Project number (RSP2024R345), King Saud University, Riyadh. Saudi Arabia.

Appendix A. Supplementary data

Supplementary data to this article can be found online at <https://doi.org/10.1016/j.jksus.2024.103466>.

References

- Ahmed, A., Usman, M., Yu, B., et al., 2020. Efficient photocatalytic degradation of toxic Alizarin yellow R dye from industrial wastewater using biosynthesized Fe nanoparticle and study of factors affecting the degradation rate. *J. Photochem. Photobiol. B*. 202, 111682. <https://doi.org/10.1016/j.jphotobiol.2019.111682>.
- Al-Farraj, E.S., Alhabarah, A.N., Ahmad, J., et al., 2018. Fabrication of hybrid nanocomposite derived from chitosan as efficient electrode materials for supercapacitor. *Int. J. Biol. Macromol.* 120 (Pt B), 2271–2278. <https://doi.org/10.1016/j.ijbiomac.2018.08.104>.
- Alfryyan, N., Kordy, M.G.M., Abdel-Gabbar, M., et al., 2022. Characterization of the biosynthesized intracellular and extracellular plasmonic silver nanoparticles using *Bacillus cereus* and their catalytic reduction of methylene blue. *Sci. Rep.* 12 (1), 12495. <https://doi.org/10.1038/s41598-022-16029-1>.
- Alzoubi, G.M., 2022. Observation of spin-glass-like behavior over a wide temperature range in single-domain nickel-substituted cobalt ferrite nanoparticles. *Nanomaterials (Basel)* 12 (7). <https://doi.org/10.3390/nano12071113>.
- Bagade, A.A., Ganbavle, V.V., Mohite, S.V., et al., 2017. Assessment of structural, morphological, magnetic and gas sensing properties of CoFe(2)O(4) thin films. *J. Colloid. Interface. Sci.* 497, 181–192. <https://doi.org/10.1016/j.jcis.2017.02.067>.
- Byun, D., Jin, Y., Kim, B., et al., 2000. Photocatalytic TiO(2) deposition by chemical vapor deposition. *J. Hazard. Mater.* 73 (2), 199–206. [https://doi.org/10.1016/s0304-3894\(99\)00179-x](https://doi.org/10.1016/s0304-3894(99)00179-x).
- Chirgwin, H., Cairncross, S., Zehra, D., et al., 2021. Interventions promoting uptake of water, sanitation and hygiene (WASH) technologies in low- and middle-income countries: An evidence and gap map of effectiveness studies. *Campbell. Syst. Rev.* 17 (4), e1194.
- Chung, S., Zhang, M., 2021. Microwave-assisted synthesis of carbon dot - iron oxide nanoparticles for fluorescence imaging and therapy. *Front. Bioeng. Biotechnol.* 9, 711534. <https://doi.org/10.3389/fbioe.2021.711534>.
- Devarajan, S., Bera, P., Sampath, S., 2005. Bimetallic nanoparticles: a single step synthesis, stabilization, and characterization of Au-Ag, Au-Pd, and Au-Pt in sol-gel derived silicates. *J. Colloid. Interface. Sci.* 290 (1), 117–129. <https://doi.org/10.1016/j.jcis.2005.04.034>.
- Dhayalan, M., Denison, M.L.J., Ayyar, M., et al., 2018. Biogenic synthesis, characterization of gold and silver nanoparticles from *Coleus forskohlii* and their clinical importance. *J. Photochem. Photobiol. B*. 183, 251–257. <https://doi.org/10.1016/j.jphotobiol.2018.04.042>.
- Dippong, T., Toloman, D., Lazar, M.D., et al., 2023. Effects of lanthanum substitution and annealing on structural, morphologic, and photocatalytic properties of nickel ferrite. *Nanomaterials (Basel)* 13 (24). <https://doi.org/10.3390/nano13243096>.
- Hajdu, V., Sikora, E., Kristaly, F., et al., 2022. Palladium decorated, amine functionalized Ni-, Cd- and Co-ferrite nanospheres as novel and effective catalysts for 2,4-dinitrotoluene hydrogenation. *Int. J. Mol. Sci.* 23 (21). <https://doi.org/10.3390/ijms232113197>.
- He, Y., Dai, C., Zhou, X., 2017. Magnetic cobalt ferrite composite as an efficient catalyst for photocatalytic oxidation of carbamazepine. *Environ. Sci. Pollut. Res. Int.* 24 (2), 2065–2074. <https://doi.org/10.1007/s11356-016-7978-1>.
- Jara, Y.S., Mekiso, T.T., Washe, A.P., 2024. Highly efficient catalytic degradation of organic dyes using iron nanoparticles synthesized with *Vernonia Amygdalina* leaf extract. *Sci. Rep.* 14 (1), 6997. <https://doi.org/10.1038/s41598-024-57554-5>.
- Khoso, W.A., Haleem, N., Baig, M.A., et al., 2021. Synthesis, characterization and heavy metal removal efficiency of nickel ferrite nanoparticles (NFN's). *Sci. Rep.* 11 (1), 3790. <https://doi.org/10.1038/s41598-021-83363-1>.
- Koul, B., Poonia, A.K., Yadav, D., et al., 2021. Microbe-mediated biosynthesis of nanoparticles: applications and future prospects. *Biomolecules*. 11 (6). <https://doi.org/10.3390/biom11060886>.
- Laghrib, F., Ajermoun, N., Bakasse, M., et al., 2019. Synthesis of silver nanoparticles assisted by chitosan and its application to catalyze the reduction of 4-nitroaniline. *Int. J. Biol. Macromol.* 135, 752–759. <https://doi.org/10.1016/j.ijbiomac.2019.05.209>.
- Leonel, A.G., Mansur, A.A.P., Carvalho, S.M., et al., 2021. Tunable magnetothermal properties of cobalt-doped magnetite-carboxymethylcellulose ferrofluids: smart nanoplatforms for potential magnetic hyperthermia applications in cancer therapy. *Nanoscale. Adv.* 3 (4), 1029–1046. <https://doi.org/10.1039/d0na00820f>.
- Londono-Calderon, C.L., Moscoco-Londono, O., Muraca, D., et al., 2017. Synthesis and magnetic properties of cobalt-iron/cobalt-ferrite soft/hard magnetic core/shell nanowires. *Nanotechnology*. 28 (24), 245605. <https://doi.org/10.1088/1361-6528/aa7010>.
- Masuku, M., Nure, J.F., Atagana, H.I., et al., 2024. Advancing the development of nanocomposite adsorbent through zinc-doped nickel ferrite-pinecone biochar for removal of chromium (VI) from wastewater. *Sci. Total. Environ.* 908, 168136. <https://doi.org/10.1016/j.scitotenv.2023.168136>.
- McMullan, G., Meehan, C., Conneely, A., et al., 2001. Microbial decolourisation and degradation of textile dyes. *Appl. Microbiol. Biotechnol.* 56 (1–2), 81–87. <https://doi.org/10.1007/s002530000587>.
- Nam, J., Won, N., Jin, H., et al., 2009. pH-Induced aggregation of gold nanoparticles for photothermal cancer therapy. *J. Am. Chem. Soc.* 131 (38), 13639–13645. <https://doi.org/10.1021/ja902062j>.
- Passero, A., Ferreira, K.M., Diniz, M.F., et al., 2024. Quantification of natural rubber blends by reflection/reflectance infrared and confocal Raman spectroscopy: a comparison of statistical methods. *An. Acad. Bras. Cienc.* 96 (3), e20230387.
- Patil, D.J., Behera, S.N., 2023. Synthesis and characterization of nanoparticles of cobalt and nickel ferrites for elimination of hazardous organic dyes from industrial wastewater. *Environ. Sci. Pollut. Res. Int.* 30 (18), 53323–53338. <https://doi.org/10.1007/s11356-023-26059-5>.
- Pedone, L., Caponetti, E., Leone, M., et al., 2005. Synthesis and characterization of CdS nanoparticles embedded in a polymethylmethacrylate matrix. *J. Colloid. Interface. Sci.* 284 (2), 495–500. <https://doi.org/10.1016/j.jcis.2004.10.019>.
- Prathna, T.C., Chandrasekaran, N., Raichur, A.M., et al., 2011. Biomimetic synthesis of silver nanoparticles by Citrus limon (lemon) aqueous extract and theoretical prediction of particle size. *Colloids. Surf. B. Biointerfaces*. 82 (1), 152–159. <https://doi.org/10.1016/j.colsurfb.2010.08.036>.
- Ranjithkumar, V., Hazeen, A.N., Thamilselvan, M., et al., 2014. Magnetic activated carbon-Fe3O4 nanocomposites—synthesis and applications in the removal of acid yellow dye 17 from water. *J. Nanosci. Nanotechnol.* 14 (7), 4949–4959. <https://doi.org/10.1166/jnn.2014.9068>.
- Sadeghi, R., Sharifi, A., Orłowska, M., et al., 2020. Investigation of Microwave Absorption Performance of CoFe(2)O(4)/NiFe(2)O(4)/Carbon Fiber Composite Coated with Polypyrrole in X-Band Frequency. *Micromachines. (base)* 11 (9). <https://doi.org/10.3390/mi11090809>.
- Sarkar, J., Mollick, M.M., Chattopadhyay, D., et al., 2017. An eco-friendly route of gamma-Fe(2)O(3) nanoparticles formation and investigation of the mechanical properties of the HPMC-gamma-Fe(2)O(3) nanocomposites. *Bioprocess. Biosyst. Eng.* 40 (3), 351–359. <https://doi.org/10.1007/s00449-016-1702-x>.
- Shanmugam, J., Dhayalan, M., Savaas Umar, M.R., et al., 2022. Green synthesis of silver nanoparticles using *Allium cepa* var. *aggregatum* natural extract: antibacterial and cytotoxic properties. *Nanomaterials (Basel)* 12 (10). <https://doi.org/10.3390/nano12101725>.
- Sofronie, M., Popescu, B., Enculescu, M., et al., 2022. Processing effects on the martensitic transformation and related properties in the Ni(55)Fe(18)Nd(2)Ga(25) ferromagnetic shape memory alloy. *Nanomaterials. (base)* 12 (20). <https://doi.org/10.3390/nano12203667>.
- Tandon, R., Tandon, N., Patil, S.M., 2021. Overview on magnetically recyclable ferrite nanoparticles: synthesis and their applications in coupling and multicomponent reactions. *RSC. Adv.* 11 (47), 29333–29353. <https://doi.org/10.1039/d1ra03874e>.
- Tiekink, E.R., 2002. Gold derivatives for the treatment of cancer. *Crit. Rev. Oncol. Hematol.* 42 (3), 225–248. [https://doi.org/10.1016/s1040-8428\(01\)00216-5](https://doi.org/10.1016/s1040-8428(01)00216-5).
- Vorobyova, M., Biffoli, F., Giurlani, W., et al., 2023. PVD for decorative applications: a review. *Materials. (base)* 16 (14). <https://doi.org/10.3390/ma16144919>.
- Wang, J., Zhang, Q., Shao, X., et al., 2018. Properties of magnetic carbon nanomaterials and application in removal organic dyes. *Chemosphere*. 207, 377–384. <https://doi.org/10.1016/j.chemosphere.2018.05.109>.
- Wu, H., Liu, G., Wang, X., et al., 2011. Solvothermal synthesis of cobalt ferrite nanoparticles loaded on multiwalled carbon nanotubes for magnetic resonance imaging and drug delivery. *Acta. Biomater.* 7 (9), 3496–3504. <https://doi.org/10.1016/j.actbio.2011.05.031>.
- Yelgaonkar, S.P., Campillo-Alvarado, G., MacGillivray, L.R., 2020. Phototriggered Guest Release from a Nonporous Organic Crystal: Remarkable Single-Crystal-to-Single-Crystal Transformation of a Binary Cocrystal Solvate to a Ternary Cocrystal. *J. Am. Chem. Soc.* 142 (49), 20772–20777. <https://doi.org/10.1021/jacs.0c09732>.
- Zeynizadeh, B., Mohammadzadeh, I., Shokri, Z., et al., 2017. Synthesis and characterization of NiFe(2)O(4)@Cu nanoparticles as a magnetically recoverable catalyst for reduction of nitroarenes to arylamines with NaBH(4). *J. Colloid. Interface. Sci.* 500, 285–293. <https://doi.org/10.1016/j.jcis.2017.03.030>.
- Zou, C., Yang, B., Bin, D., et al., 2017. Electrochemical synthesis of gold nanoparticles decorated flower-like graphene for high sensitivity detection of nitrite. *J. Colloid. Interface. Sci.* 488, 135–141. <https://doi.org/10.1016/j.jcis.2016.10.088>.